Unidirectional Current Flow and Charge State Trapping at Redox Polymer Interfaces on Bilayer Electrodes: Principles, Experimental Demonstration, and Theory

P. Denisevich, K. W. Willman, and Royce W. Murray*

Contribution from the Kenan Laboratories of Chemistry, University of North Carolina, Chapel Hill, North Carolina 27514. *Received January 30, 1981*

Abstract: Bilayer electrodes consist of conducting electrodes coated with or bonded to two physically discrete polymeric layers which contain two different redox substances having different $E^{\circ\prime}$ values. The redox substance in the inner polymeric film next to the electrode can be oxidized or reduced by the electrode. That in the outer polymer film is constrained, by physical isolation from the electrode, to undergo oxidation or reduction only at electron energies for redox conductivity by the inner film. This arrangement leads to rectified (unidirectional) current flow. Experimental results from bilayer electrodes based on nine different combinations of redox substances in the films are presented to demonstrate the generality of the phenomenon and the ability to fabricate bilayer films. The redox substances include fixed-site redox polymers like poly[Ru(4-methyl-4′-vinyl-2,2′-bipyridine)$_3$]$^{2+}$, polyvinylferrocene, poly(4-methyl-4′-vinyl-*N*,*N*′-ethylene-2,2′-bipyridinium), and a siloxane polymer of *N*-methyl-*N*′-(4-(2-(trimethoxysilyl)ethyl)benzyl)-4,4′-bipyridinium, and (inner film) mobile redox sites like bromide, hexachloroiridate, and benzoquinone. Various mechanisms are considered for bilayer electrode nonidealities which appear as leakage of redox state trapped in the outer film, and a theory describing voltammetric properties of bilayer electrodes is compared to experimental results.

The unidirectional, or rectifying, flow of electrons across the interface between two substances, where one or both are semiconductor materials, is a familiar phenomenon highly exploited by current solid-state electronics technology. The unidirectional electron flow is seated in gradients of potential which accompany carrier depletion or space-charge layers in the semiconductor. In chemistry, the rectifying characteristics of semiconductor/electrolyte solution interfaces have been the focus of much recent research in photoelectrochemistry.[1]

This laboratory recently proposed[2] a new principle of unidirectional electron flow across an interface, which does not rely upon semiconductor characteristics or space-charge effects. The interface is that between two ultrathin films, each containing a redox substance, the two-layer (or *bilayer*) film assembly being contacted on one side by a conductor electrode and on the other by an electrolyte solution (or a second electrode). The films employed were polymeric forms of the complexes [Ru(2,2′-bipyridine)$_2$(4-vinylpyridine)$_2$](ClO$_4$)$_2$ and [Ru(2,2′-bipyridine)$_2$(4-vinylpyridine)Cl](ClO$_4$), assembled as discrete layers on a Pt electrode, first depositing a film of the first polymeric complex and over it a film of the latter, to form the bilayer. The second, outer film, isolated from the Pt electrode by the inner film, undergoes electron-transfer reactions with the electrode via electron-transfer mediation by redox states of the inner film. The resulting interface between the inner and outer polymeric films exhibits a unidirectional electron-flow property even though neither of the polymeric complexes has any known semiconductor character.

This paper will demonstrate that the above rectifying characteristic manifests a general principle of unidirectional electron flow, by illustrating the bilayer rectifying characteristic with many combinations of redox substances. The redox substances are summarized in Figure 1. The principles of bilayer electrodes are discussed in order to emphasize how these differ from the usual concepts of semiconductor interfaces. Finally, a rudimentary theory for bilayer electrodes is introduced which accounts for the unusual appearance of their electrochemical current–potential waves.

Principles of Electrochemical Action of Bilayer Electrodes

This section describes properties of two-layer[3] or bilayer films of different redox substances. The discussion is based on an illustrative bilayer electrode whose electron energy[4] level diagram is shown in Figure 2. The electrode is prepared by first coating the conductor electrode (e.g., Pt) with a thin film of electrochemically polymerized[2] [Ru(4-methyl-4′-vinyl-2,2′-bipyridine)$_3$](ClO$_4$)$_2$, poly-Ru(VB)$_3^{2+}$, as the *inner film*, and then with a film of polyvinylferrocene,[5] PVFer, as the outer film. Consider first just the inner film.

Inner Film. Redox transformations between three different oxidation states in the inner-film poly-Ru(VB)$_3^{2+}$ can be accomplished by setting the potential applied to the electrode at *a*, *b*, or *c* (Figure 2), which switches the film to the poly-Ru(VB)$_3^{3+}$, poly-Ru(VB)$_3^{2+}$, poly-Ru(VB)$_3^{+}$ states, respectively. The equivalent of many monomolecular layers of Ru(VB)$_3^{2+}$ sites becomes thus oxidized or reduced since the inner films of poly-Ru(VB)$_3^{2+}$ contain from 1×10^{-9} up to 1×10^{-7} mol/cm^2 of sites and a monomolecular layer[6] is about 8×10^{-11} mol/cm^2. Probably, only the poly-Ru(VB)$_3^{2+}$ sites nearest the electrode interface undergo direct electron-transfer reactions with it. The other, more remote sites, unable to achieve contact with the electrode, undergo oxidation and reduction by self-exchange of electrons between neighbor poly-Ru(VB)$_3^{2+}$ and poly-Ru(VB)$_3^{3+}$ sites as shown schematically at the bottom of Figure 2. This mechanism for electron transport through redox polymer films on electrodes was first proposed by Kaufman and Engler[7] and is becoming widely accepted[8,9] although its kinetic details are yet to be fully explored. The electron transport is accompanied by a charge compensating flow of anionic counterions, associated solvent, and involved polymer chain motions. Which factor(s) control the rate of electron and ion transport (i.e., electrochemical charge) need not concern us here.

The poly-Ru(VB)$_3^{2+}$ film thus has a conductivity to the flow of electrons resulting from its chemical reactivity. We dub this *redox conductivity* to distinguish it from the more familiar, but

(1) Nozik, A. J. *Annu. Rev. Phys. Chem.* **1978**, *29*, 189.

(2) (a) Abruña, H. D.; Denisevich, P.; Umaña, M.; Meyer, T. J.; Murray, R. W. *J. Am. Chem. Soc.* **1981**, *103*, 1. (b) Denisevich, P.; Abruña, H. D.; Leidner, C. R.; Meyer, T. J.; and Murray, R. W., to be submitted for publication.

(3) Three-layer film assemblies involve generally the same ideas.

(4) The potential scale of Figure 2 is equivalent to an electron energy level diagram except that a single line is used to represent a pair of redox states.

(5) Daum, P.; Murray, R. W. *J. Phys. Chem.* **1981**, *85*, 389.

(6) Abruña, H.; Meyer, T. J.; Murray, R. W. *Inorg. Chem.* **1979**, *11*, 3233.

(7) (a) Kaufman, F. B.; Engler, E. M. *J. Am. Chem. Soc.* **1979**, *101*, 547. (b) Kaufman, F. B.; Schroeder, A. H.; Engler, E. M.; Kramer, S. R.; Chambers, J. Q. *Ibid.* **1980**, *102*, 483.

(8) (a) Oyama, N.; Anson, F. C. *J. Electrochem. Soc.* **1980**, *127*, 640. (b) *Anal. Chem.* **1980**, *52*, 1192. (c) Oyama, N.; Shigehara, K.; Anson, F. C. *Inorg. Chem.* **1981**, *20*, 518. (d) Peerce, P. J.; Bard, A. J. *J. Electroanal. Chem.* **1980**, *114*, 89. (e) Degrand, C.; Miller, L. L. *J. Am. Chem. Soc.* **1980**, *102*, 5728.

(9) (a) Nowak, R. J.; Schultz, F. A.; Umaña, M.; Lam, R.; Murray, R. W. *Anal. Chem.* **1980**, *52*, 315. (b) Daum, P.; Murray, R. W. *J. Electroanal. Chem.* **1979**, *103*, 289. (c) Daum, P.; Lenhard, J. R.; Rolison, D. R.; Murray, R. W. *J. Am. Chem. Soc.* **1980**, *102*, 4649.

0002-7863/81/1503-4727$01.25/0

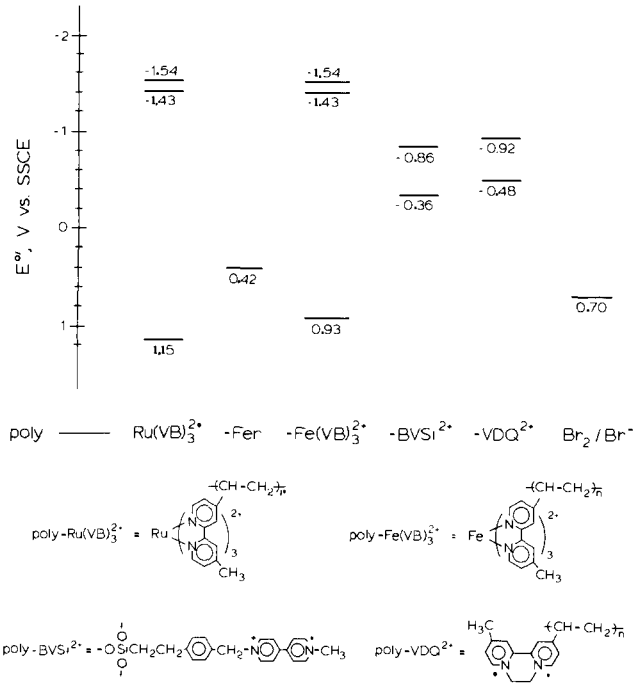

Figure 1. Formal potentials for redox couples used in this article, in CH_3CN.

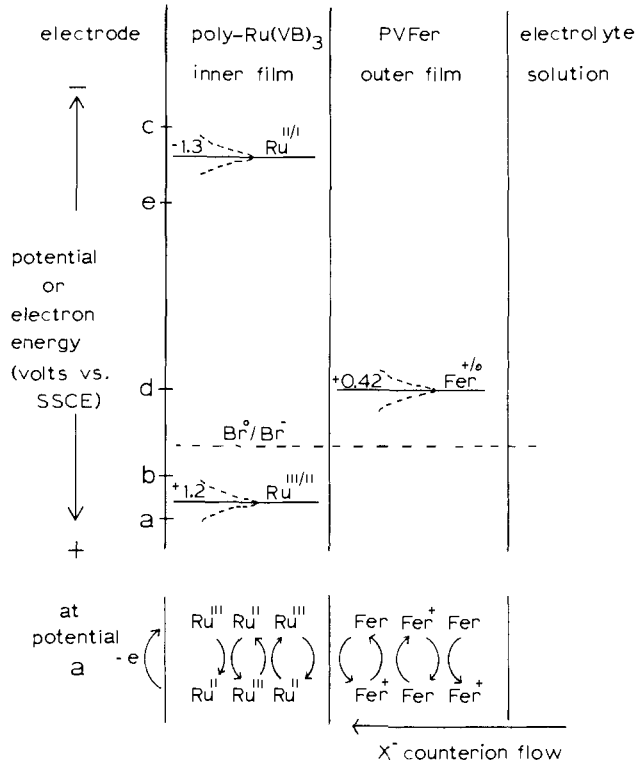

Figure 2. Schematic representation of electron energy levels for a Pt/poly-Ru(VB)$_3^{2+}$/PVFer bilayer electrode.

different, electronic conductivity, since redox conductivity permits electrons to flow *within the film* only at energies centered[10] around the formal potentials of the poly-Ru(VB)$_3^{n+}$ couples, and in redox conductivity an exhaustive chemical (redox) transformation of the film is possible. Thus, at electrode potential *d* (Figure 2), electrons (ideally) cannot cross the film of poly-Ru(VB)$_3^{2+}$ at that energy. At potential *d*, the film can act as an oxidizing surface only toward substances oxidizable at potentials more negative than ca. −1.3 V (via the poly-Ru(VB)$_3^{2+/+}$ level) and as a reducing surface only toward substances reducible at potentials more positive than ca. +1.2 V vs. SSCE (via the poly-Ru(VB)$_3^{3+/2+}$ level). For substances oxidized or reduced at intermediate potentials, the film acts as an insulator. *The constraint of conducting electrons within the film only at the energies of the film's redox levels, with insulating characteristics at other energies, is the essential characteristic of redox polymers upon which the special rectifying (and other) operation of bilayer films can be based.*

Potential gradients in the inner-film redox polymer (or in any redox polymer film on an electrode) might drive electron transport. At a naked, charged electrode in an electrolyte solution, an electrical double layer exists, the diffuse part of which contains a space charge of cations and anions attracted to (or repelled by) the electrode. The thickness of this space charge of ions and potential depends strongly upon the electrolyte concentration,[11] being approximately 10 and 100 Å in 1 and 0.01 M electrolyte, respectively. A redox polymer such as poly-Ru(VB)$_3^{2+}$ can be considered a viscous polyelectrolyte solution, containing Ru(VB)$_3^{2+}$ sites, their ClO_4^- counterions, plus supporting electrolyte ions (e.g., $Et_4N^+ClO_4^-$) from the external solution. In contact with a charged electrode, ionic accumulation and depletion occurs within this polyelectrolyte solution, just as in an electrolyte solution, although the details probably differ somewhat owing to the relative immobility of the poly-Ru(VB)$_3^{2+}$ sites (among other factors). Since the ionic concentration in the poly-Ru(VB)$_3^{2+}$ film is large, the space charge of ions and potential will be correspondingly small. Specifically, if the film contains 2×10^{-9} mol/cm^2 of poly-Ru(VB)$_3^{2+}$ sites and has a density[12] of 1.3 g/cm^3, its physical thickness is ca. 130 Å which is much thicker than the probable diffuse layer space-charge thickness. By the above argument, significant potential gradients are not expected to extend completely across the inner redox polymer film unless the film is very thin.

An ion accumulation/depletion layer should also exist at the outer boundary of the poly-Ru(VB)$_3^{2+}$ film, a situation analogous to that at the surface of an ion-exchange material. By the same reasoning as above, this interface should not be a source of potential gradients extending completely across the inner redox film.

Outer Film. Now consider electrochemical events involving the outer, polyvinylferrocene film, which has a level of redox conductivity[13] centered at the ferrocene/ferricenium formal potential. At other potentials, conductivity to electron transport is, ideally, low. Let us sequentially apply potentials *d*, *b*, *a*, *b*, *d*, *e*, *c*, and *d*, to the bilayer electrode of Figure 2, to describe the special characteristics of the interface between the two films of redox polymer.

Potential *d*. The initial state of the bilayer film is Pt/poly-Ru(VB)$_3^{2+}$/PVFer.

Potential *b*. Thermodynamically, the PVFer film should become oxidized but does not since (ideally) no mechanism exists for electron transport between the PVFer film and the electrode at this electron energy.

Potential *a*. Oxidation of inner-film polymer and transport of poly-Ru(VB)$_3^{3+}$ sites to its outer boundary leads to the rapid oxidation of the outer film PVFer by reaction 1 (Table I). This mediated electron-transfer reaction is labeled a trapping reaction. Its rate is conceivably determined by several factors. We will later set out a quantitative theoretical model for *sweeping* the electrode potential from *d* to *a* which considers the electron-exchange event at the film interface as the RDS.

(10) Since concentration ratios like [poly-Ru(VB)$_3^{3+}$]/[poly-Ru(VB)$_3^{2+}$] change according to the Nernst equation, redox transformations occur over a narrow range of electron energies not just a single, distinct value (see dotted line, Figure 2).

(11) Delahay, P. "Double Layer and Electrode Kinetics"; Interscience: New York, 1965; p 44.

(12) This is an approximate conversion, assuming[2] that film density equals bulk poly-Ru(VB)$_3^{2+}$(ClO$_4$)$_2$ density of 1.35 g/cm^3. XPS results[18] suggest (but not unambiguously) that density of very thin films may be lower, as low as 0.3 g/cm^3. The Ru(VB)$_3^{2+}$ site concentrations for these two densities would be 1.6 and 0.35 M, respectively.

(13) The rate of electron transport in PVFer has been investigated,[5,8d,9a,c] and its diffusion coefficient, obtained as $D_{ct}^{1/2}C$ where C is the concentration of redox sites, is in the range $D_{ct} = 10^{-9}$–10^{-11} cm^2/s.

Table I. Summary of Electron-Transfer Reactions Which Trap Outer Redox Polymer Film in Oxidized or Reduced State and Which Untrap These States

reaction no.	bilayer electrode, trapping and untrapping reactions	K_{eq}[a]
	Pt/poly-$Ru(VB)_3^{2+}$/PVFer	
1	trapping: poly-$Ru(VB)_3^{3+}$ + $PVFer \rightarrow$ poly-$Ru(VB)_3^{2+}$ + $PVFer^+$	2×10^{12}
2	trapping: $Br_2 + 2PVFer \rightarrow 2Br^- + 2PVFer^+$	6×10^6
3	untrapping: poly-$Ru(VB)_3^+$ + $PVFer^+ \rightarrow$ poly-$Ru(VB)_3^{2+}$ + PVFer	2×10^{32}
	Pt/poly-$Ru(VB)_3^{2+}$/poly-$Fe(VB)_3^{2+}$	
4	trapping: poly-$Ru(VB)_3^{3+}$ + poly-$Fe(VB)_3^{2+} \rightarrow$ poly-$Ru(VB)_3^{2+}$ + poly-$Fe(VB)_3^{3+}$	5×10^3
	Pt/poly-$Ru(VB)_3^{2+}$/poly-$BVSi^{2+}$	
5	trapping: 2poly-$Ru(VB)_3^+$ + poly-$BVSi^{2+} \rightarrow$ 2poly-$Ru(VB)_3^{2+}$ + poly-$BVSi^0$	2×10^{36}
6	untrapping: 2poly-$Ru(VB)_3^{3+}$ + poly-$BVSi^0 \rightarrow$ 2-poly-$Ru(VB)_3^{2+}$ + poly-$BVSi^{2+}$	10^{51}
7	untrapping: Br_2 + poly-$BVSi^0 \rightarrow 2\,Br^-$ + poly-$BVSi^{2+}$	8×10^{39}
	Pt/poly-$Ru(VB)_3^{2+}$/poly-VDQ^{2+}	
8	trapping: 2poly-$Ru(VB)_3^+$ + poly-$VDQ^{2+} \rightarrow$ poly-$Ru(VB)_3^{2+}$ + poly-VDQ^0	1×10^{32}
9	trapping: $BQ^{-\cdot}$ + poly-$VDQ^{2+} \rightarrow$ BQ + poly-VDQ^+	10^1
10	untrapping: 2poly-$Ru(VB)_3^{3+}$ + poly-$VDQ^0 \rightarrow$ 2poly-$Ru(VDQ)_3^{2+}$ + poly-VDQ^{2+}	10^{55}
	Pt/poly-VDQ^{2+}/PVFer	
11	trapping: $Br_2 + 2PVFer \rightarrow 2Br^- + 2PVFer^+$	6×10^6
12	$IrCl_6^{2-}$ + $PVFer \rightarrow IrCl_6^{3-}$ + $PVFer^+$	3×10^6
13	untrapping: poly-VDQ^+ + $PVFer^+ \rightarrow$ poly-VDQ^{2+} + PVFer	2×10^{15}

[a] For the trapping reaction (1), for example, $(RT/n_{ch}F)\ln K_{eq} = (E^0_{in} - E^0_{out})$ or $\log K_{eq} = (1.15 - 0.42)/0.059$. K_{eq} calculated from $E^{\circ\prime}$ values of Figure 1.

Since reaction 1 has a large K_{eq}, application of potential *a* for a sufficient time should quantitatively oxidize both inner and outer films (to poly-$Ru(VB)_3^{3+}$ and $PVFer^+$), resulting in a flow of electrochemical charge equivalent to the combined total of electroactive sites in the two redox polymers, i.e., $\Gamma_{Ru} + \Gamma_{Fe}$. (In practice, by applying potential *a* only for a short time or by sweeping the potential only partly from *b* toward *a* and then reversing the sweep, it should be possible to oxidize a large fraction of the outer film to $PVFer^+$ but very little of the inner film.)

Potential *b*: current flows to reduce poly-$Ru(VB)_3^{3+}$ sites.

Potential *d*. Nothing further happens. At this point, although it should (thermodynamically) become reduced, the outer film is *trapped* in the $PVFer^+$ state by the inability of the inner film to support electron transport at this potential. (One recognizes that various nonidealities, or *leakage* pathways, for electron flow, will eventually allow reduction of trapped $PVFer^+$. Experiment and theory for the leakage topic are taken up later.)

Note that in the above progression of potentials, current (and charge equivalent to Γ_{Fe}) was passed across the inner/outer-film interface *unidirectionally. The rectifying action of the inner/outer-film interface is attributable to the existence of discrete levels of redox conductivity plus insulating regions as in Figure 2 and should therefore be a general property of redox polymer film bilayers* with analogous electron energy level structures. The rectifying action does *not* depend on the existence of bent bands or space-charge effects as is the case at semiconductor/electrolyte interfaces and is fundamentally different from that situation. We offer the scheme of redox polymer bilayers (and multilayers) as a novel avenue to the design of rectifying electrochemical interfaces and devices.

Potential *e*. Ideally, there is no change in the $PVFer^+$ trapped state although the thermodynamic imbalance between electrode and outer film is now large.

Potential *c*. At this potential, poly-$Ru(VB)_3^+$ sites are electrochemically generated in the inner film; these migrate to the inner/outer-film boundary to reduce the $PVFer^+$ trapped states in the outer film, in the *untrapping reaction* (*3*) (Table I). This reaction has a large K_{eq}, ensuring complete reduction of the outer film and passage of electrochemical charge, if both films are completely reduced (which is not essential), equivalent to $\Gamma_{Ru} + \Gamma_{Fe}$. The theoretical description of the rate of the untrapping reaction is equivalent to that for the trapping reaction, as discussed later.

Potential *d*. At this potential, the inner film is reoxidized to the poly-$Ru(VB)_3^{2+}$ state and the film has been reset to its initial condition. Note that the overall potential excursion required to oxidize and rereduce the outer film is (ideally) 1.15 + 1.30 = 2.45 V. In the process, energy was *stored in the outer film*, 0.73 V being released in reaction 1 and 1.72 V being released in reaction 3. Energy-storage aspects of the bilayer electrode assembly have several connotations, including storage of charge for memory or power purposes and for population of excited states[14] during the outer-film-trapping electron-exchange reaction.

Mobile Species in the Film. Ions and neutral molecules which partition into the polymer film assembly from the external electrolyte solution can play important roles in bilayer electrode operation.

1. Ion Flow for Inner-Film Oxidation-State Change. The trapping reaction (1) alters fixed-site charges in the inner film, from poly-$Ru(VB)_3^{2+}$ to poly-$Ru(VB)_3^{3+}$, which requires a charge compensating flow *through the outer film* of either supporting electrolyte anions into or cations out of the inner film. The ambient concentration of these ions and their mobilities in the outer film must be adequate to support this ion flux or else inner-film electrochemistry and thus outer-film oxidation-state trapping (and untrapping) may become kinetically retarded. Such a situation might result if the material chosen for the outer film contained fixed anionic sites, for instance.

2. Redox Conductivity Bands Provided by Mobile Redox Couples. Ions or neutral species permeating the inner redox polymer film which themselves are members of reversible redox couples form new levels of redox conductivity across the inner film and provide alternative electron-transport routes to the outer film. For instance, the horizontal dotted line at 0.82 V in Figure 2 corresponds to Br_2/Br^-. Bromide added to the external electrolyte solution should partition into the inner poly-$Ru(VB)_3^{2+}$ film, and at potential *b* should be oxidized to Br_2 at the electrode/poly-$Ru(VB)_3^{2+}$ interface. The Br_2 oxidant, transported to the in-

(14) Consider for instance the case where the outer film has a luminescing or usefully reactive excited state at an energy less negative than the $Ru^{II/I}$ potential.

ner/outer-film interface either by diffusion or by electron self-exchange with bromide in the inner film, oxidizes outer-film PVFer sites and yields a new trapping electron exchange, reaction 2 (Table I).

Advantages as to economy and simplicity of chemical materials, their stability and ease of replenishment, and flexible choice of operating potentials for the inner redox film may result by using mobile redox sites such as the Br_2/Br^- couple. Note also that reaction 2 renders the poly-$Ru(VB)_3^{3+}$ oxidation state superfluous for the PVFer trapping reaction. One could analogously employ a mobile redox couple with formal potential $-1.3 < E^\circ < +0.4$ V appropriate for untrapping outer-film $PVFer^+$. In principle, in fact, the inner polymer film of a bilayer electrode need bear *no fixed redox sites at all* but instead simply be permeable to and support the electron transport of dissolved redox couples. Stable, ultrathin ion-exchange or zeolitic materials could thus be considered for inner-film layers.

3. Film Assembly. The permeability of the inner film toward other substances is of concern during application of the outer redox polymer film. While it is perhaps not essential that the inner/outer-film interface be physically sharply defined, intermingling of outer-film redox sites into the inner film carries the danger of those sites achieving contact with the electrode surface for electron flow directly to the outer film at its own E°, a leakage pathway to be avoided.

Two experimental strategies have been employed to avoid catastrophic intermingling during outer-film application. One approach uses outer-film materials already in the polymerized state, e.g., polyvinylferrocene, and relies on the typically slow interdiffusion of one polymer into another. The second strategy is based on polymerizing the outer film from solutions of cationic monomers onto the preformed polymeric, fixed-cation site, inner film, and depends upon charge exclusion from the inner polymer to prevent intrusion of monomer.

One-Layer Films Containing Mixtures of Redox Substances. We[2] and Anson[15] have shown that films of copolymers of redox monomers and random mixtures of redox polymers exhibit electrochemical reactions at the characteristic potentials of the two individual redox components. The proportions of the redox components used in these mixtures studies have been not far from 1:1. In this circumstance, each redox constituent has sufficiently close like neighbors that self-exchange of electrons with those neighbors, and therefore electron transport, remains fast on the experimental time scale throughout the entire film. Consider on the other hand, a redox mixture where one redox couple is a sufficiently dilute constituent so that the flux of its *electron self-exchange reactions with like but now distant neighbors is slow.* (This situation should be especially achievable in a cross-linked random copolymer.) In this case, electrochemical reactivity of the dilute redox component sites remote from the electrode could be quenched on the voltammetric time scale. These sites could however become oxidized or reduced at potentials where the majority redox constituent is oxidized or reduced, the latter acting as an electron transfer mediator. (A proposed experimental illustration of this is included in this paper.) Electrochemical properties resulting from this mediation formally resemble those expected of a physically segregated bilayer electrode, although, theoretically, details of trapping reactions in a homogeneous mixture differ from those at interfaces. Trapping of redox states of highly diluted redox components should aid the study of electron-transfer distance–rate effects.

Experimental Examples of Bilayer Electrodes

The preceding was an "in principle" discussion of an idealized bilayer electrode. The principles now need experimental demonstration, including evidence that assembly of bilayers is reducible to more general practice than proved by our early example.[2] One could reasonably argue that it is difficult to stably arrange ultrathin films of electrochemically reversible redox polymers in good electron-transfer contact with the electrode (the inner film), with each other (the rectifying interface), and with the outer film spatially segregated from the electrode. Described below are six different bilayer electrode assemblies, using ten different combinations of redox materials, nine of which exhibit many characteristics of the ideal bilayer. We begin with the example of Figure 2.

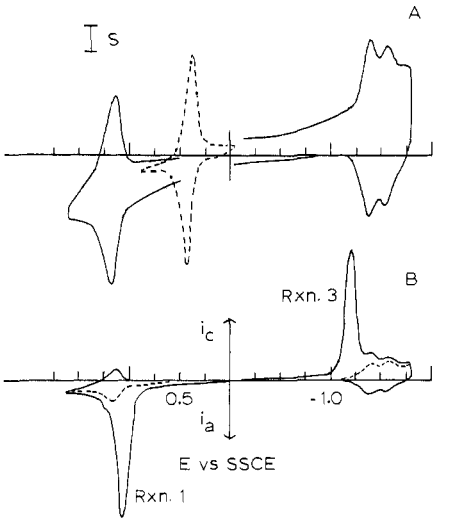

Figure 3. Cyclic voltammetry of (curve A) Pt/poly-$Ru(VB)_3^{2+}$ (solid line) one-layer electrode at 0.1 V/s, S = 46 $\mu A/cm^2$, and Pt/PVFer (dashed line) one-layer at 0.1 V/s, S = 91 $\mu A/cm^2$, both 4×10^{-9} mol/cm^2, and (curve B) Pt/poly-$Ru(VB)_3^{2+}$/PVFer bilayer where $\Gamma_{Ru} = 2.4 \times 10^{-9}$ and $\Gamma_{Fe} = 1.2 \times 10^{-8}$ mol/cm at 0.1 V/s, S = 227 $\mu A/cm^2$. Solid line represents $0 \rightarrow +1.6 \rightarrow -1.6 \rightarrow$ 0-V potential excursion. Dashed line represents results if scan reversed at 0.6 V or (for the negative potential region) if the virgin scan was $0 \rightarrow -1.6 \rightarrow$ 0-V (all in 0.1 M Et_4NClO_4/CH_3CN).

Pt/Poly-$Ru(VB)_3^{2+}$/PVFer Bilayer Electrode. Poly-$Ru(VB)_3^{2+}$ films prepared by electrochemical polymerization[2] from $Ru(VB)_3^{2+}$ monomer solutions are convenient for bilayer assembly. Film coverage can be prescribed, and the well-defined, stable, poly-$Ru(VB)_3^{2+}$ cyclic voltammetry (illustrated for a one-layer film in Figure 3, curve A) is reproducible. The surface waves occur at formal potentials close to those of dissolved monomer as is also the case for a one-layer film of PVFer, curve A (dashed line). These waves arise solely from the surface films; the solutions here (and throughout unless specified otherwise) contain only supporting electrolyte.

A Pt/poly-$Ru(VB)_3^{2+}$/PVFer bilayer electrode is shown in Figure 3, curve B. An initial $0 \rightarrow -1.6 \rightarrow$ 0-V potential scan (dashed line, cathodic; solid line, anodic) displays reversible poly-$Ru(VB)_3^{2+/+}$ and poly-$Ru(VB)_3^{+/0}$ waves identical with those on the one-layer Pt/poly-$Ru(VB)_3^{2+}$ electrode. This observation is significant, showing that ingress and egress of ions necessary for the reductive electrochemistry of the inner-film poly-$Ru(VB)_3^{2+}$ is not unduly disturbed by the outer-film PVFer.[16]

If the potential applied to the Pt/poly-$Ru(VB)_3^{2+}$/PVFer electrode is now swept $0 \rightarrow +1.6 \rightarrow 0$ V, no wave appears (at any time) at +0.42 V vs. SSCE, the normal potential for PVFer oxidation and rereduction. Instead, on the virgin $0 \rightarrow +1.6$-V sweep, a large sharp current peak occurs at a potential on the leading edge of the wave for poly-$Ru(VB)_3^{2+}$ oxidation. According to the discussion of Figure 2, this current should represent the outer-film oxidation by trapping reaction 1 (Table I). Reversing the potential scan, $+1.6 \rightarrow 0$ V, yields a cathodic wave at 1.15 V vs. SSCE for rereduction of inner-film poly-$Ru(VB)_3^{3+}$, but no reverse peak occurs at the potential of the trapping peak or at that for the reduction of outer-film $PVFer^+$ states, at any potential scan rate. This trapping of the outer film in its oxidized $PVFer^+$ state is the rectifying property ideally expected if the inner

(15) Oyama, N.; Anson, F. C. *J. Am. Chem. Soc.* **1979**, *101*, 3450.

(16) This is consistent with the well-defined one-layer Pt/PVFer electrochemistry in acetonitrile (Figure 3), since if solvent did not swell and supporting electrolyte ions did not permeate the initially neutral PVFer layer, severe ohmic resistance distortion would result.

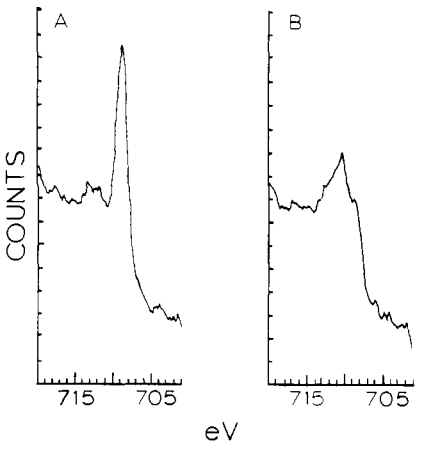

Figure 4. XPS of a Pt/poly-Ru(VB)$_3^{2+}$/PVFer bilayer with (curve A) no electrochemical pretreatment and after (curve B) a 0 → +1.6 → −0.74-V potential excursion, maintaining the −0.74-V potential for 1 min before disconnecting the electrode.

poly-Ru(VB)$_3^{2+}$ film has no electron-transport conductivity between +0.4 and 0 V. *It is easily reproduced from bilayer electrode to bilayer electrode.*

The stability of the trapped outer-film PVFer$^+$ state is demonstrated by the following. If following the above 0 → +1.6 → 0-V potential excursion, a second positive excursion is initiated immediately, from 0 V vs. SSCE, only the voltammetric pattern for inner-film poly-Ru(VB)$_3^{2+}$ is observed (curve B, dashed line, Figure 3). If the second potential scan is initiated after a wait of 18 min at −0.65 V vs. SSCE, a small peak reappears at the trapping peak potential but with an amplitude <10% of the original. Not only does the outer-film PVFer$^+$ trapping persist at a potential 1.1 V more negative than (thermodynamically) required for its reduction but also it does so nearly quantitatively. For this remarkable result, the rate of loss, or leakage, of PVFer$^+$ sites in the outer film was $<2 \times 10^{-13}$ mol/s of sites or a reductive current of <20 nA. The *effective* resistance of the inner film (at −0.65 V relative to +0.42 V vs. SSCE) was 5×10^7 Ω. Not only does current flow unidirectionally through the poly-Ru(VB)$_3^{2+}$/PVFer interface to trap PVFer$^+$ but also the trapped state film acts as a remarkably *low-leakage electrochemical capacitor.*

An XPS experiment provided direct proof that the outer film becomes stably oxidized in the reaction 1 trapping peak of Figure 3, curve B. Figure 4A shows the sharp Fe $2p_{3/2}$ band of outer-film PVFer (no prior electrochemistry) at a binding energy of 708.5 eV characteristic[17] of ferrocene. If a bilayer electrode is scanned (0 → +1.6 → −0.7 V) through the trapping wave and the potential held at −0.74 V vs. SSCE for 1 min, then disconnected, washed, and air-dried, panel B (Figure 4) shows that the Fe $2p_{3/2}$ band of this trapped-state electrode now lies at 710.3 eV and is broadened, both characteristics[17] of ferricenium XPS. No obvious peak for PVFer is seen in panel B, although the broadness of the PVFer$^+$ band makes quantitation difficult. Note that due to the XPS surface selectivity, panel B corresponds to PVFer$^+$ sites on the outermost boundary of the outer film, e.g., the sites most remote from the electrode.

As anticipated in the discussion of Figure 2, trapped outer-film PVFer$^+$ can be untrapped via reduction of the inner film. Thus, following a 0 → +1.6 → 0-V potential excursion, a 0 → −1.6 → 0-V continuation of the potential scan causes a sharp reduction current peak (Figure 3B) on the leading edge of the poly-Ru(VB)$_3^{2+/+}$ wave, followed by the poly-Ru(VB)$_3^{2+/+}$ and poly-Ru(VB)$_3^{+/0}$ waves. The sharp reduction current peak is thought to be the untrapping reaction 3, which returns the outer film to the PVFer state. In accord with this, the peak is absent on a second 0 → −1.6 → 0-V potential excursion (dashed curve), and a reaction 1 outer-film trapping peak at ca. +1.08 V vs. SSCE which is identical to the virgin one now reappears in a 0 → +1.6 → 0-V potential excursion.

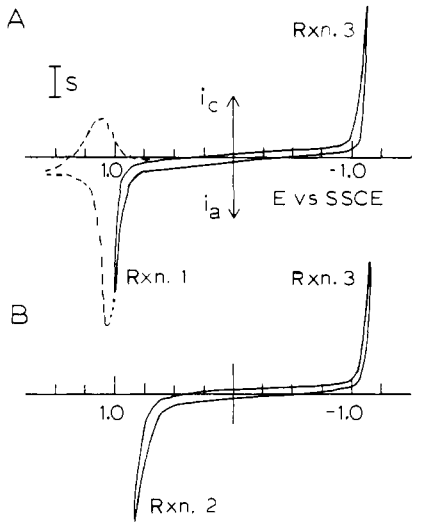

Figure 5. Steady-state cyclic voltammetry of Pt/poly-Ru(VB)$_3^{2+}$/PVFer bilayer electrode of Figure 3 where (curve A, solid line) potential scan limits are abbreviated and (curve B) ~2 mM bromide is added to 0.1 M Et_4NClO_4/CH_3CN (0.1 V/s, S = 91 μA/cm^2).

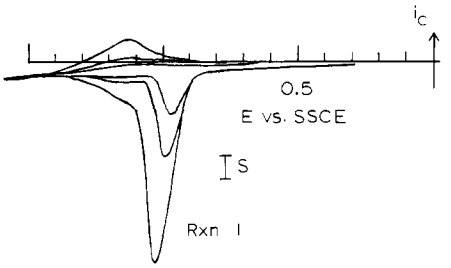

Figure 6. Cyclic voltammetry of Pt/poly-Ru(VB)$_3^{2+}$/PVFer bilayer electrode of Figure 3B where v = 10, 20, 50 mV/s, S = 91 μA/cm^2, 0.1 M Et_4NClO_4/CH_3CN.

The potentials of the reaction 1 trapping and reaction 3 untrapping peaks in Figure 3 are well separated from those of the poly-Ru(VB)$_3^{2+}$ oxidation and reduction waves, respectively. The redox conductivity of the inner-film poly-Ru(VB)$_3^{2+}$ is high; only a small fraction of the inner-film redox sites need become oxidized or reduced for effective electron transport to/from the outer film. (For the case shown in Figure 3, the peak current for the trapping reaction occurs ca. 80 mV negative of $E°$ for the $Ru^{3+/2+}$ couple. At this potential only about 4% of the inner film is in the Ru^{3+} state.) This feature of the Pt/poly-Ru(VB)$_3^{2+}$/PVFer bilayer, emphasized in the abbreviated cyclical scan of Figure 5 (curve A), can be of practical utility when the inner film has chemically fragile oxidation states, as for example inner-film Ru(VB)$_3^+$ in wet or acidic solvents. It is also notable that repetitive trapping and untrapping of outer film is possible in a *steady-state* current–potential pattern. The shape of the current–potential pattern in Figure 5A suggests contemplation of how the rectifying properties of bilayer electrodes might usefully mimic solid-state electronic devices.

Dissolved redox species such as Br^-, which partitions into the poly-Ru(VB)$_3^{2+}$ inner film and is more easily oxidized than poly-Ru(VB)$_3^{2+}$ sites, provide an alternative redox conductivity pathway for oxidative trapping (reaction 2) of outer-film PVFer$^+$, as illustrated in Figure 5 (curve B), where anodic current rises sharply at ca. +0.7 V vs. SSCE for the generation of bromine and thus outer-film PVFer$^+$, spawning the subsequent cathodic current peak for untrapping outer-film PVFer$^+$ (reaction 3). The stable cyclical current–potential pattern is again diode-like.

(17) (a) Lenhard, J. R.; Murray, R. W. *J. Am. Chem. Soc.* **1978**, *100*, 7870. (b) Fischer, A. B.; Wrighton, M. S.; Umaña, M.; Murray, R. W. *Ibid.* **1979**, *101*, 3442. (c) Umaña, M.; Rolison, D. R.; Nowak, R.; Daum, P.; Murray, R. W. *Surf. Sci.* **1980**, *101*, 295.

(18) Umaña, M.; Denisevich, P.; Rolison, D. R.; Nakahama, S.; Murray, R. W. *Anal. Chem.* **1981**, *53*, 1170.

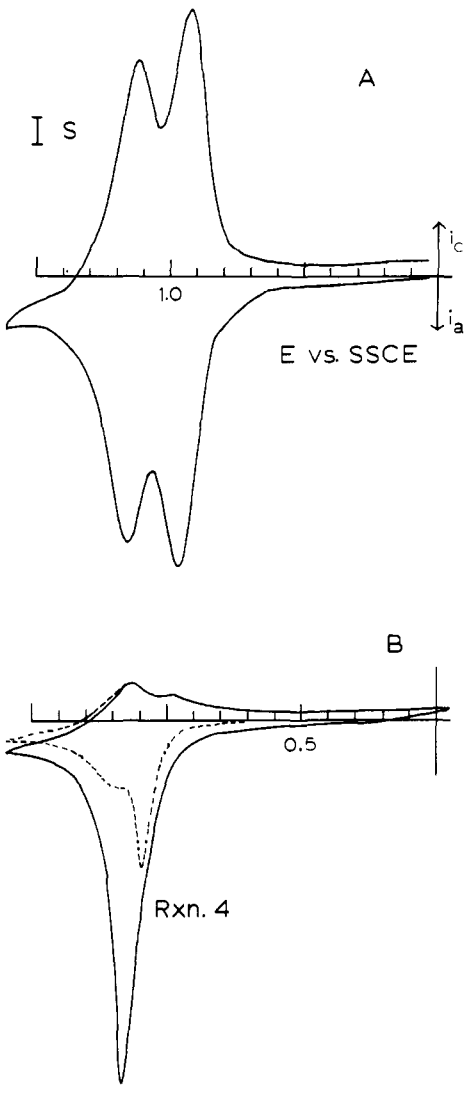

Figure 7. Cyclic voltammetry of (curve A) Pt/copoly-$Fe(VB)_3^{2+}$–$Ru(VB)_3^{2+}$ at 0.05 V/s, S = 25 μA/cm^2, and of (curve B) Pt/poly-$Ru(VB)_3^{2+}$/poly-$Fe(VB)_3^{2+}$ bilayer electrode where $\Gamma_{Ru} = 1 \times 10^{-8}$ and $\Gamma_{Fe} = 3.5 \times 10^{-8}$ mol/cm^2 at 0.1 V/s, S = 100 μA/cm^2. Solid line represents initial 0 → +1.6 → 0-V potential excursion; dashed line is immediately repeated 0 → +1.6 → 0-V.

Bilayer electrode cyclic voltammograms depend on the potential scan rate and on coverages of inner (Γ_{Ru}) and outer (Γ_{Fe}) redox films. With increasing scan rate, the leading edges of both outer-film trapping and untrapping current peaks rise together (Figure 6), and the peak potentials move systematically toward those of the poly-$Ru(VB)_3^{3+/2+}$ and poly-$Ru(VB)_3^{2+/+}$ reactions, respectively. A bilayer with larger Γ_{Ru} exhibits less prominent trapping and untrapping peaks, a consequence of relative quantity. Finally, a decrease in Γ_{Fe} (not shown) causes the trapping and untrapping peak potentials to move away from those of the poly-$Ru(VB)_3^{3+/2+}$ and poly-$Ru(VB)_3^{2+/+}$ reactions. These variations are anticipated by theory (discussed later).

The application of one polymeric substance, PVFer, as an overlayer upon a probably highly cross-linked film (poly-$Ru(VB)_3^{2+}$) was calculated to introduce minimal intermingling of the two polymers. The results above show that this strategy was highly successful, as nearly ideal bilayer characteristics were observed. The practical minimum coverage of inner-film poly-$Ru(VB)_3^{2+}$ has not been established. Such limiting phenomena are under investigation.

Pt/Poly-Ru(VB)$_3^{2+}$/Poly-Fe(VB)$_3^{2+}$ Bilayer Electrode. The electrochemistry of (concurrently electropolymerized) one-layer, copolymer films of Pt/copoly-$Fe(VB)_3^{2+}$–$Ru(VB)_3^{2+}$ is a simple summation[2] of that of one-layer Pt/poly-$Ru(VB)_3^{2+}$ and Pt/poly-$Fe(VB)_3^{2+}$ films. The $M^{3+/2+}$ formal potentials differ by 215 mV (Figure 7, curve A). On an electrode already coated with a film of Pt/poly-$Ru(VB)_3^{2+}$, a solution of $Fe(VB)_3^{2+}$ does not exhibit an anodic wave at its usual potential but rather is electrocatalytically oxidized at the potential for Pt/poly-$Ru(VB)_3^{2+}$ oxidation.

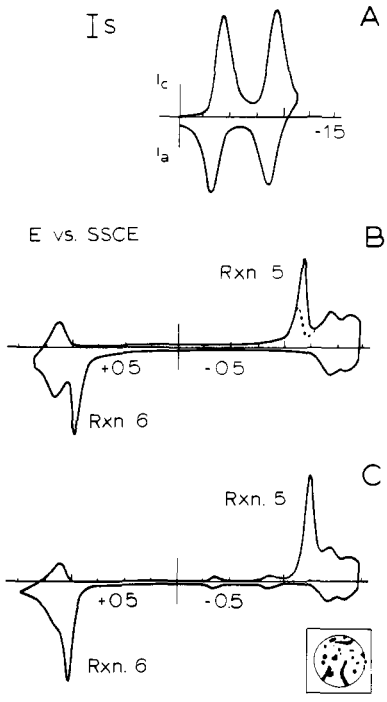

Figure 8. Cyclic voltammetry of (curve A) Pt/poly-$BVSi^{2+}$ one-layer electrode, $\Gamma_{BVSi} = 4 \times 10^{-8}$ mol/cm^2, at 0.1 V/s, S = 200 μA/cm^2, and of (curve B) Pt/poly-$Ru(VB)_3^{2+}$/poly-$BVSi^{2+}$ bilayer electrode where $\Gamma_{Ru} = 2.3 \times 10^{-9}$ and $\Gamma_{BVSi} = 2 \times 10^{-9}$ mol/cm^2 at 0.2 V/s, S = 250 μA/cm^2. Solid line represents 0 → −1.8 → +1.5 → 0-V potential excursion. Dashed line is a second 0 → −1.8 → 0-V scan 3 min (at 0 V) after a 0 → −1.8 → 0-V potential scan. Curve C: pinholed bilayer where ca. 15% of naked Pt is exposed (inset shows pinhole pattern), 0 → −1.8 → +1.6 → 0-V scan at 0.2 V/s, S = 100 μA/cm^2 (all in 0.1 M Et_4NClO_4/CH_3CN).

Since the $Fe(VB)_3^{2+}$ seems to be excluded from the Pt/poly-$Ru(VB)_3^{2+}$ film, reductively polymerizing $Fe(VB)_3^{2+}$ on a Pt/poly-$Ru(VB)_3^{2+}$ electrode should produce a spatially segregated bilayer electrode. XPS angular distribution measurements confirm this,[2a] and the thus prepared bilayer electrode exhibits the sharp anodic current peak expected for outer-film trapping (reaction 4, Table I; Figure 7, curve B). Outer-film trapping of poly-$Fe(VB)_3^{3+}$ states is however consistently "leaky" and thus imperfect. This is evidenced by a cathodic wave at the potential for poly-$Fe(VB)_3^{3+}$ reduction and by the reappearance of a trapping reaction peak in an immediately repeated 0 → +1.6 → 0-V potential scan (dashed line).

The leaky discharge of outer-film Pt/poly-$Ru(VB)_3^{2+}$/poly-$Fe(VB)_3^{3+}$ states stands in sharp contrast to the remarkable stability of trapped outer-film Pt/poly-$Ru(VB)_3^{2+}$/$PVFer^+$ states. The small equilibrium constant of reaction 4, only 5×10^3, seems the most likely explanation for the leakiness. A theoretical model, discussed later, suggests that the difference between formal potentials of the inner and outer redox systems is important in designing stably trapping bilayer electrodes.

Pt/Poly-Ru(VB)$_3^{2+}$/Poly-BVSi^{2+} Bilayer Electrode. One-layer films of poly(benzylviologen silane), poly-$BVSi^{2+}$ (see Experimental Section) exhibit[19] well-formed waves (Figure 8, curve A) in acetonitrile for reaction 14. According to Figure 1, an outer

$$\underset{\text{colorless}}{\text{poly-BVSi}^{2+}} \underset{-e^-}{\overset{e^-}{\rightleftharpoons}} \underset{\text{blue}}{\text{poly-BVSi}^{+}} \underset{-e^-}{\overset{e^-}{\rightleftharpoons}} \underset{\text{yellow}}{\text{poly-BVSi}^{0}} \quad (14)$$

film of poly-$BVSi^{2+}$ on a Pt/poly-$Ru(VB)_3^{2+}$ electrode should become reductively trapped as $BVSi^0$. (The preceding trapping reactions were oxidations.) This trapping reaction involves two

electrons and traps a color state as well as an oxidation state.

The cyclic voltammogram of a Pt/poly-Ru(VB)$_3^{2+}$/poly-BVSi^{2+} bilayer in which $\Gamma_{Ru} \approx \Gamma_{BVSi}$ is shown in Figure 8 (curve B). An initial 0 → +1.5 → 0-V potential excursion (not shown) reveals a normal poly-Ru(VB)$_3^{2+}$ oxidation wave, indicating the outer-film poly-BVSi^{2+} layer allows adequate counterion mobility. A 0 → −1.8 → 0-V potential sweep shows no waves at the viologen potentials so the inner-film poly-Ru(VB)$_3^{2+}$ has no redox conductivity at these electron energies. A sharp reduction current peak appears at ca. −1.2 V vs. SSCE, on the leading edge of the wave producing poly-Ru(VB)$_3^{+}$ which should be outer-film trapping reaction 5 (Table I). This wave, entirely absent on an immediately repeated 0 → −1.8 → 0-V potential excursion, is quantitatively reproduced following a 0 → +1.5 → 0-V potential scan in which making poly-Ru(VB)$_3^{3+}$ untraps (reaction 6, Table I) the outer-film poly-BVSi^{0} in a sharp anodic peak as shown in Figure 8 (curve B). Outer-film poly-BVSi^{0} can alternatively be untrapped by bromide oxidation (reaction 7, not shown). These are all ideally expected bilayer properties.

For investigation of the stability of the trapped outer-film poly-BVSi^{0}, the electrode of Figure 8B was, after trapping of the outer film, held at 0 V vs. SSCE for 3 min, and a second 0 → −1.8 → 0-V potential scan was performed. As shown by the dashed section of curve B, some of the outer film became discharged, resulting in a retrapping peak about 30% as large as the original one. This corresponds to a leakage current of about 65 nA or a flux of 6.7×10^{-12} mol/cm^2 s of viologen sites becoming reoxidized by one electron. This is a larger leakage rate than the Pt/poly-Ru(VB)$_3^{2+}$/PVFer bilayer and unlike the latter tended to fluctuate from experiment to experiment. A likely reason for at least part of this leakage is traces of oxygen dissolved in the electrolyte. (In confirmation of our supposition about oxygen, if the leakage experiment is carried out in a controlled atmosphere box, the leakage rate was observed to drop to 7×10^{-13} mol/cm^2 s.) One calculates that chemical discharge by oxygen diffusing to the bilayer electrode, to yield the above results, requires only ca. 6×10^{-6} and 0.6×10^{-6} M trace oxygen, respectively.

We propose that the above sensitivity to traces of reactive impurities in the solution should have analytical advantages, providing with a given bilayer system the rate of other sources of outer-film trapped state leakage either is known or is small.

Although the bilayer trapping and (especially) untrapping reaction peaks tend to be broadened (Figure 9A), it was possible to prepare the poly-Ru(VB)$_3^{2+}$/BVSi^{2+} bilayer on highly doped, optically transparent SnO_2 electrodes. This permitted a spectral evaluation of outer-film BVSi^{0} trapping stability. Figure 9B shows the optical absorbance[20] of a SnO_2/poly-Ru(VB)$_3^{2+}$/poly-BVSi^{2+} bilayer as a function of time and applied potential, at 400 nm, the λ_{max} of poly-BVSi^{0}. Pulsing the potential to −1.6 V for 30 s causes a large, rapid absorbance increase, only a part of which (that due to poly-Ru(VB)$_3^{0}$) vanishes upon returning the potential to 0 V. The remaining absorbance, thought to be due to trapped poly-BVSi^{0}, corresponds (for $\epsilon = 2 \times 10^4$) to a trapped outer-film coverage of 4×10^{-9} mol/cm^2 of poly-BVSi^{0} sites, which compares reasonably well with the coverage of 3.4×10^{-9} mol/cm^2 of poly-BVSi^{2+} present on this bilayer. The 400-nm absorbance in this experiment was very stable (oxygen having been successfully excluded), persisting for 30 min as shown (leakage rate $<10^{-13}$ mol/cm^2 s). The bilayer and the yellow coloration of the electrode could be discharged by a brief potential pulse to +1.8 V vs. SSCE, generating poly-Ru(VB)$_3^{3+}$ sites.

We thought that pinholes in the inner film, leading to direct electron transfer between electrode and outer film, might be fatal to the bilayer rectifying property. The following experiment was illuminating in this regard. Pinholes were artificially created in a Pt/poly-Ru(VB)$_3^{2+}$ inner film by dotting a naked Pt electrode with Apiezon grease spots, carrying out the poly-Ru(VB)$_3^{2+}$ coating step, and then washing the electrode with hexane to remove the Apiezon dots, exposing ca. 15% (by visual inspection) of the underlying Pt. The poly-BVSi^{2+} film was then applied. On this bilayer (Figure 8, curve C), *both* direct poly-BVSi^{2+} reduction waves and outer-film trapping current peaks (reaction 5) are

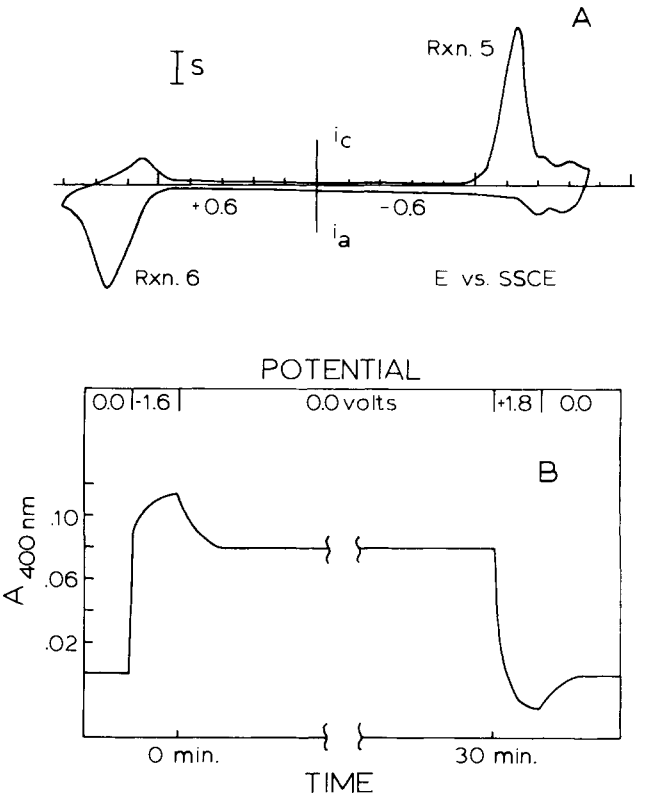

Figure 9. Curve A: cyclic voltammetry of a SnO_2/poly-Ru(VB)$_3^{2+}$/poly-BVSi^{2+} bilayer electrode where $\Gamma_{Ru} = 1.1 \times 10^{-9}$ and $\Gamma_{BVSi} = 3.4 \times 10^{-9}$ mol/cm^2, 0 → −1.8 → +1.6 → 0-V scan at 0.1 V/s, S = 100 μA/cm^2. Curve B: absorbance at 400 nm of a SnO_2/poly-Ru(VB)$_3^{2+}$/poly-BVSi^{2+} prepared as above except $\Gamma_{Ru} = 4 \times 10^{-9}$ mol/cm^2, at indicated potentials (all in 0.1 M Et_4NClO_4/CH_3CN).

observed, presumably through the artificial pinholes and on the normally bilayered regions of the electrode, respectively. This experiment is valuable, demonstrating that pinholes produce current leaks but do not cause a general "shorting out" of the bilayer film. The inference that the rate of lateral electron transport through the inner film from pinhole regions is slow is in fact understandable in that electrochemical charge appears to diffuse through redox polymers[5,8d,9] with D_{ct} = ca. 10^{-9} cm^2/s. At this diffusion rate, reduced poly-BVSi^{0} sites would migrate only about 10^{-3} cm from the edge of a pinhole in 10^3 s.

Pt/Poly-Ru(VB)$_3^{2+}$/Poly-VDQ^{2+} Bilayer Electrode. Vinyldiquat, VDQ^{2+}, can be electropolymerized[19] at −1.2 V vs. SSCE on a naked Pt electrode, producing stable, adherent viologen polymer films with surface waves even more symmetrically defined than those of poly-BVSi^{2+} in Figure 8A. Electropolymerization also proceeds smoothly by reduction of VDQ^{2+} monomer by the Pt/poly-Ru(VB)$_3^{+}$ or poly-Ru(VB)$_3^{0}$ surface,[21] producing an adherent outer film with the distinctive bilayer electrode response shown in Figure 10 (curve A). The sharp trapping and untrapping current peaks are strikingly well-defined and correspond to reactions 8 and 10 (Table I). Overall behavior of the Pt/poly-Ru(VB)$_3^{2+}$/poly-VDQ^{2+} bilayer is similar to that of the Pt/poly-Ru(VB)$_3^{2+}$/poly-BVSi^{2+} bilayer, and explanation of the experimental features will not be repeated.

It is easy to incrementally add small amounts of outer-film poly-VDQ^{2+} to the Pt/poly-Ru(VB)$_3^{2+}$/poly-VDQ^{2+} bilayer by repeated reduction of the film in a solution of the VDQ^{2+} monomer. Figure 10 (inset) illustrates this to show that currents

(19) Willman, K. W., University of North Carolina, 1980, to be submitted for publication.

(20) Inspection of spectra of one-layer SnO_2/poly-Ru(VB)$_3^{2+}$ and SnO_2/poly-BVSi^{2+} electrodes shows that absorbance at 400 nm on the bilayer is governed by the presence of BVSi^{0}.

(21) VDQ^{2+} monomer does not penetrate the Pt/poly-Ru(VB)$_3^{2+}$ film during polymerization as shown by the absence of reduction waves at the normal VDQ^{2+} potentials.

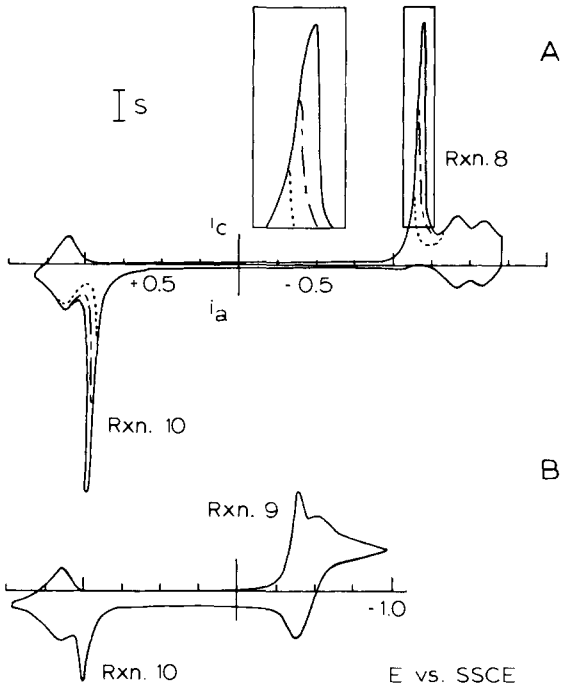

Figure 10. Cyclic voltammetry of Pt/poly-Ru(VB)$_3^{2+}$/poly-VDQ^{2+} bilayer electrode where (curve A) $\Gamma_{Ru} = 4.3 \times 10^{-9}$ and $\Gamma_{VDQ} \approx 1.5 \times 10^{-9}$ (---), $\sim 4 \times 10^{-9}$ (-·-), and $\sim 7 \times 10^{-9}$ mol/cm^2 (—), by incremental deposition of poly-VDQ^{2+}, 0 → −1.8 → +1.6 → 0-V potential scan at 0.1 V/s, S = 250 μA/cm^2, and where (curve B) $\Gamma_{Ru} = 10^{-9}$ and $\Gamma_{VDQ} = 7 \times 10^{-9}$ mol/cm^2 and 0.1 mM benzoquinone is added to the 0.1 M Et_4NClO_4/CH_3CN, 0 → −1.0 → +1.6 → 0-V potential at 0.1 V/s, S = 250 μA/cm^2.

for the reductive trapping peak *rise together* and their peak potentials systematically shift to more negative values as the coverage of outer-film poly-VDQ^{2+} increases. The same effects are observed by increasing the potential scan rate. These features are theoretically anticipated as discussed later.

The Pt/poly-Ru(VB)$_3^{2+}$/poly-VDQ^{2+} bilayer is relatively nonleaky as compared to the analogously prepared (electropolymerized outer film) Pt/poly-Ru(VB)$_3^{2+}$/poly-Fe(VB)$_3^{2+}$ bilayer. This reinforces our belief that leakiness of the latter bilayer arises from the small K_{eq} of its trapping reaction (as noted above) rather than imperfection in the spatial segregation of the bilayer films.

The poly-VDQ^{2+} outer film is trapped by inner-film poly-Ru(VB)$_3^{+}$ in a two-electron reduction. So that the outer film could be trapped instead as poly-VDQ^{+}, the negative potential scan could be abbreviated so as to allow passage of only a one-electron amount of charge or a mobile inner-film reductant could be chosen which has a potential interposed between the two viologen waves. The latter tactic is demonstrated by adding *p*-benzoquinone (Figure 10, curve B) to the solution, which has the desired effect of shifting the sharp current trapping peak to a more positive value. This peak, corresponding to trapping reaction 9, just precedes the reversible wave for reduction of the quinone to its radical anion and in fact occurs at a potential very near the thermodynamic poly-VDQ$^{2+/+}$ potential. The poly-VDQ^{+} trapping is, as expected, consequently leaky.

Pt/Poly-VDQ^{2+}/PVFer Bilayer Electrode. The preceding bilayer electrodes were based on inner-film poly-Ru(VB)$_3^{2+}$. To show that bilayer electrode responses are general phenomena and are not peculiar to the use of this particular inner-film polymer, we deposited a polyvinylferrocene film evaporatively on a Pt/poly-VDQ^{2+} electrode. In Et_4NClO_4/acetonitrile medium, the poly-VDQ^{2+} waves are observable at their usual potentials, but the outer-film PVFer layer is electrochemically silent, since the poly-VDQ^{2+} inner film has no sufficiently oxidizing potential for redox conductivity. Bromide was employed therefore for the PVFer^{+} trapping reaction. As shown in Figure 11 (curve A), a 0 → +0.85 → −0.8 → 0-V potential scan, producing Br_2 in the initial positive excursion, does oxidatively trap (reaction 11)

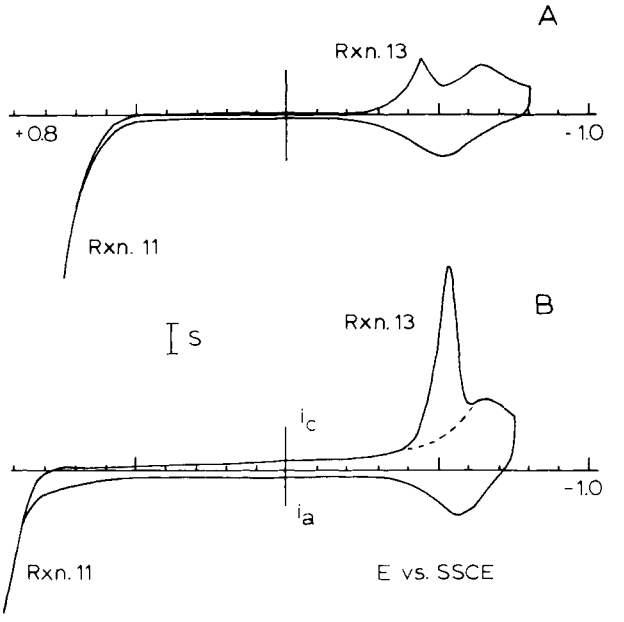

Figure 11. Cyclic voltammetry of Pt/poly-VDQ^{2+}/PVFer bilayer electrode where (curve A) $\Gamma_{VDQ} = 4 \times 10^{-9}$ and $\Gamma_{PVFer} = 1 \times 10^{-9}$ mol/cm^2 in 0.1 M Et_4NClO_4/CH_3CN containing bromide, 0 → +0.85 → −0.80 → 0-V potential scan at 0.1 V/s, S = 200 μA/cm^2 and (curve B) $\Gamma_{VDQ} = 4 \times 10^{-9}$ and $\Gamma_{PVFer} = 4.3 \times 10^{-9}$ mol/cm^2 in aqueous 0.2 M $LiClO_4$/pH 7 phosphate buffer containing a small amount of NaBr. Solid curve is 0 → +1.0 → −0.75 → 0-V potential scan; dashed curve is +0.6 → −0.75 V.

outer-film PVFer^{+} as evidenced by the ensuing untrapping current peak at ca. −0.45 V (reaction 13) on the leading edge of the poly-VDQ^{2+} reduction wave. This untrapping peak is only observed following the Br_2-producing positive excursion and shifts to more negative potentials at higher potential sweep rates in the same fashion as the other bilayers.

The Pt/poly-VDQ^{2+}/PVFer bilayer electrode can furthermore be employed in an aqueous medium containing bromide (Figure 11, curve B). The trapping–untrapping sequence can be repeated many times in both solvents although the poly-VDQ$^{2+/+}$ wave exhibits an increased peak potential separation, indicating that the PVFer layer offers some resistance to counterion motion. The excellent insulating properties of the poly-VDQ^{2+} toward electron transport at the PVFer potential were demonstrated by potentiostating a Pt/poly-VDQ^{2+}/PVFer bilayer (with outer-film untrapped) at 0.6 V vs. SSCE (sufficient thermodynamically to oxidize PVFer) for 30 min. The degree of PVFer outer-film oxidation was then assessed by a negative (untrapping) potential sweep, which as seen in Figure 11 (curve B, dashed line) produced no detectable PVFer^{+} untrapping peak. With the assumption that 1×10^{-10} mol/cm^2 of trapped PVFer^{+} could have been detected, this result translates to an oxidation current for PVFer^{+} production at −0.6 V of <5 nA/cm^2 or $< 5 \times 10^{-14}$ mol/(cm^2 s).

Finally, to emphasize the flexibility of using mobile redox species in bilayers, we substituted a solution of $IrCl_6^{3-}$ for the bromide medium. The $IrCl_6^{3-}$ was strongly partitioned into the anion-exchanger poly-VDQ^{2+} inner film, and following a potential scan into its oxidation region (reaction 12) one can observe an outer-film PVFer^{+} untrapping reaction 13 current peak which strongly resembles those in Figure 11.

Pt/Poly-Ru(VB)$_3^{2+}$ Electrodes. Electrodes coated with films of this polymer and of the analogous poly-Fe(VB)$_3^{2+}$ and poly-Ru(bpy)$_2$(vinylpy)$_2^{2+}$ polymers[2] often exhibit small, sharply defined peaks preceding the poly-Ru(VB)$_3^{2+}$ oxidation and the poly-Ru(VB)$_3^{2+}$ reduction waves (Figure 12). The sharp reduction peak surprisingly has the characteristics of an outer-film bilayer trapping reaction peak. Namely, it occurs only on a virgin negative potential scan and is not repeated (dashed curve) unless the potential is scanned through its oxidative counterpart (which occurs between +0.8 and +1.1 V vs. SSCE) or through the po-

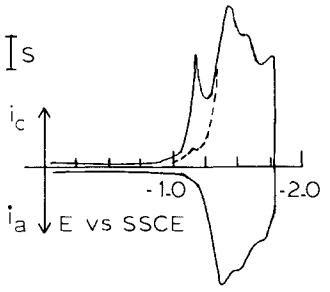

Figure 12. Cyclic voltammetry of Pt/poly-$Ru(VB)_3^{2+}$ one-layer electrode showing anomalous peak (S = 250 $\mu A/cm^2$, 0.1 M Et_4ClO_4/CH_3CN): (—) first negative sweep; (---) second negative sweep without prior anodic sweep.

tentials for bromide oxidation or ferrocene oxidation when those mobile redox species are added to the solution. The sharp peak for the oxidative counterpart likewise appears only on a virgin positive potential scan and is not repeated unless the potential is scanned through the wave of Figure 12. The potential of the sharp oxidation and reduction peaks move to progressively more positive and negative values with increasing sweep rates, respectively.

This bilayer mimicking phenomenon is curious since no deliberate steps were taken in the polymerization of $Ru(VB)_3^{2+}$ to generate either another species with different formal potential or with any element of spatial segregation within the polymer film. The phenomenon is peculiar to the metal–bpy complex systems and is *not* seen with PVFer films or viologen films or with the Pt/poly-viologen/bilayers. The size of peaks like that in Figure 12 varies from day to day; typically it is 5–10% the size of the main poly-$Ru(VB)_3^{2+}$ wave. Its magnitude is definitely enhanced by repeated scanning through the poly-$Ru(VB)_3^{2+}$ reduction waves.

We believe that the bilayer imitating peak in Figure 12 originates from a small concentration of reductively altered poly-$Ru(VB)_3^{2+}$ sites which remain electroactive and have a redox potential more negative than +0.4 V vs. SSCE (by the ferrocene untrapping result). Although we cannot rule out a spatial segregation of these electroactive "decay sites", it seems more likely that they would be more or less dispersed throughout the poly-$Ru(VB)_3^{2+}$ host film. Assuming the latter to be the case, we postulate that in the heavily cross-linked poly-$Ru(VB)_3^{2+}$, neighboring "decay sites" are too distant from one another to undergo effective self-exchange on the cyclic voltammetric time scale. (Note that a "decay site" concentration of 0.08 M (5% of the poly-$Ru(VB)_3^{2+}$ site concentration) corresponds to a very considerable 34-Å center-to-center average spacing.) Mediated oxidation or reduction of the decay sites by the host $Ru(VB)_3^{2+}$ lattice should produce bilayer-like current peaks as in Figure 12. If this postulate is correct, it represents an example of the "dilute mixture" case discussed in an earlier section of this paper.

Finally, we should note that current peaks like that in Figure 12 are presumably present in bilayer electrode responses when poly-$Ru(VB)_3^{2+}$ is used as the inner film but, owing to the much greater quantity of outer-film trapped sites, cannot account for the bilayer trapping and untrapping phenomena described above.

Theory of Electrochemical Action of Bilayer Electrodes

Trapping Reactions. In comparison to other electrocatalytic phenomena known for modified electrodes, bilayer electrode trapping and untrapping peaks are unusual for their sharp definition and for being split away from the mediator (inner-film) wave. For development of a theoretical framework for bilayer electrode trapping reaction current peaks, a choice must be made among the possible current controlling steps: (i) oxidation of inner-film sites at the Pt/polymer interface, (ii) transport of electrochemical charge through the inner and (iii) outer film, and (iv) electron transfer between inner-film and outer-film sites, e.g., a trapping reaction electron exchange such as reaction 1. Process i is likely to be very fast.[22] At slow cyclic voltammetric potential scan rates in acetonitrile solvent, peak currents for one-layer films of poly-$Ru(VB)_3^{2+}$, PVFer, poly-VDQ^{2+}, and poly-$BVSi^{2+}$ are proportional to potential scan rates, meaning that charge-transport processes ii and iii are rapid in these films on such time scales. For these reasons, theory which takes the trapping reaction, process iv, as the RDS was of interest.

When a trapping reaction for outer-film oxidation is written as eq 15, the anodic trapping current $i_{T,a}$ for outer-film oxidation

$$\text{inner (ox)} + \text{outer (red)} \rightleftharpoons \text{inner (red)} + \text{outer (ox)} \qquad (15)$$

is governed by $d\Gamma_{out(red)}/dt$, for which we write the rate law (16),

$$i_{T,a}/n_{ch}FA = -d\Gamma_{out(red)}/dt = k_{interf}\Gamma_{in(ox)}^{interf}\Gamma_{out(red)}^{interf} \qquad (16)$$

where n_{ch} is the number of electrons passed in reaction 15, Γ_{in}^{interf} and Γ_{out}^{interf} represent the quantities (mol/cm^2) of inner- and outer-film redox sites in contact at the inner/outer-film interface, and k_{interf} is the rate constant (cm^2/(mol s)) for electron-exchange there. The interface constituents are assumed to be in equilibrium with the remainder of the inner and outer films, respectively, so

$$\Gamma_{in(ox)}^{interf} = \Gamma_{in(ox)}[\Gamma_{in(ox)(t=0)}^{interf}/\Gamma_{in(t=0)}] \qquad (17)$$

$$\Gamma_{out(red)}^{interf} = \Gamma_{out(red)}[\Gamma_{out(red)(t=0)}^{interf}/\Gamma_{out(t=0)}] \qquad (18)$$

where $\Gamma_{in(t=0)}$ and $\Gamma_{out(t=0)}$ are Γ_T quantities if the films are initially in their completely oxidized and reduced forms, respectively. The ratio $\Gamma_{in(ox)}/\Gamma_{in(red)}$ in the inner film is assumed to be controlled by the electrode potential via the Nernst equation (or in more precise calculations by a modification of the Nernst equation which accounts for site interaction activity effects by including an interaction parameter, r).[23] Combining the above equations yields a relation for current when the electrode potential is swept through the trapping peak.

$$i_{T,a} = -n_{ch}FAk_{interf}\Gamma_{in(ox)(t=0)}^{interf}\Gamma_{out(red)(t=0)}^{interf}\left\{1 + \exp\left[-\frac{nF}{RT}E^\circ\right]\right\}^{p}\left\{1 + \exp\left[\frac{nF}{RT}(E - E^\circ)\right]\right\}^{(-1-p)}\left\{\exp\left[\frac{nF}{RT}(E - E^\circ)\right]\right\} \qquad (19)$$

where

$$p = \frac{RT}{nFv}\frac{k_{interf}\Gamma_{in(ox)(t=0)}^{interf}\Gamma_{out(red)(t=0)}^{interf}}{\Gamma_{out(t=0)}} \qquad (20)$$

and v is the potential sweep rate in volts/second and $E^\circ = E^\circ_{in}$. The peak potential for the trapping peak is given by

$$E_p = E^\circ_{in} - \frac{RF}{nF}\ln p \qquad (21)$$

with a peak current, for the fast trapping condition $k_{interf}\Gamma_{in(t=0)}^{interf} \gg nFv/RT$

$$i_{p,a} = -\frac{nn_{ch}AF^2v\Gamma_{out(t=0)}}{eRT} \qquad (22)$$

Equation 22 is loosely analogous to that for an irreversible thin-layer electrochemical reaction.[24]

Examples of current peaks calculated from eq 19 are shown in Figure 13A. As the experimental time scale is increased (smaller v) or equivalently as the trapping reaction rate constant k_{interf} increases, the trapping reaction peak potential (for oxidation) moves away from E°_{in} and the wave assumes a symmetrical shape, E_p shifts 59 mV per decade of v, and i_p/v becomes constant (i.e., eq 22). When the trapping reaction is slow (or the experimental time scale is fast, large v), the current peak shows an extended, descending tail and its $E_{1/2}$ ($i_{T,a}$ at $i_{p,a}/2$) lies at E°_{in}.

Equations 19–21 are approximate when site interaction activity effects (which typically broaden surface waves) are appreciable. We have investigated such cases, using numerical solutions to the

(22) Brown, A. P.; Anson, F. C. *J. Electroanal. Chem.* **1978**, *92*, 133.

(23) (a) Brown, A. P.; Anson, F. C. *Anal. Chem.* **1977**, *49*, 1589. (b) Smith, D. F.; Willman, K.; Kuo, K.; Murray, R. W. *J. Electroanal. Chem.* **1979**, *95*, 217.

(24) Hubbard, A. T. *J. Electroanal. Chem.* **1969**, *22*, 165.

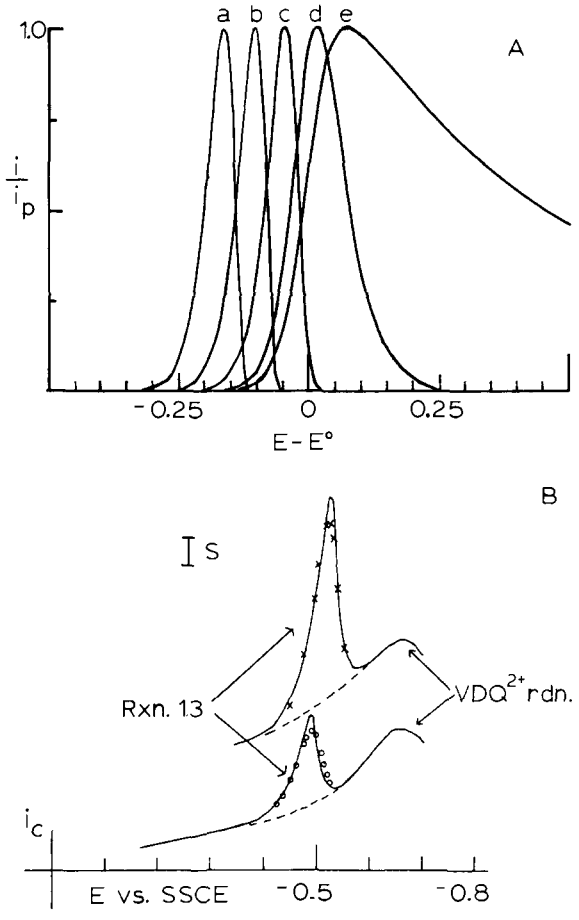

Figure 13. A: Trapping currents calculated from eq 19. Curves a–e correspond to values of p of 514, 51.4, 5.14, 0.514, and 0.0514, respectively. (E.g., curve a corresponds to v = 1 mV/s, k_{interf} = 10^{12} cm^2/(mol s), $\Gamma_{in(t=0)}^{interf} = \Gamma_{out(t=0)}^{interf} = 2 \times 10^{-10}$ mol/cm^2, $\Gamma_{out(t=0)} = 2 \times 10^{-9}$ mol/cm^2; curves b–e represent tenfold increases in v.) B: Fit of calculated and experimental currents for Pt/poly-VDQ^{2+}/PVFer electrode (reaction 13) ($\Gamma_{poly\text{-}VDQ^{2+}} = 4 \times 10^{-9}$ mol/cm^2, v = 100 mV/s, S = 100 μA/cm^2). (×) $\Gamma_{PVFer} = 4.3 \times 10^{-9}$ mol/cm^2, best-fit $k_{interf} = 1 \times 10^{14}$ cm^2/(mol s). (○) $\Gamma_{PVFer} = 1.8 \times 10^{-9}$ mol/cm^2, best-fit $k_{interf} = 1.2 \times 10^{14}$ cm^2/(mol s). Both assume $\Gamma_{in(t=0)}^{interf} = \Gamma_{out(t=0)}^{interf} = 2 \times 10^{-10}$ mol/cm^2.

equations, and find that a negative interaction parameter (r) does not change the qualitative trapping peak appearance but has the following quantitative effects: E_p tends to be more removed from $E°_{ln}$ and E_p dependency on potential sweep rate increases from 59 mV per decade at very small v to >100 mV at large v (or at slow trapping rate, small k_{interf}).

Untrapping Reactions. The theoretical relations for an untrapping reaction exactly mirror those of the trapping reaction, except for sign changes needed to represent cathodic currents. Values of k_{interf} of course are not necessarily the same for trapping and untrapping steps.

Comparison of Theory and Experiment. The trapping reaction theory predicts that a current peak for bilayer outer-film trapping reactions should preceed and be distinct from the inner-film oxidation wave (Figure 13A). This result qualitatively accounts for the bilayer electrode responses seen in Figures 3 and 5–11. The following represents a preliminary test of quantitative aspects of the theory.

(1) For oxidative trapping reaction 1 in Pt/poly-Ru(VB)$_3^{2+}$/PVFer bilayers, $i_{p,a}/v$ was constant to within ca. 15% and E_p varied as 0.090 log v and as 0.075 log v in data taken for two different electrodes over the ranges 10–100 and 1–20 mV/s, respectively.

(2) For the two-electron trapping reaction 8 in Pt/poly-Ru(VB)$_3^{2+}$/poly-VDQ^{2+} bilayers, $i_{p,c}/v$ was constant to within ca. 20% and E_p varied as 0.100 log v for v = 20–500 mV/s (electrode of Figure 10A).

(3) At the slowest potential scan rates, the observed values of trapping reaction peak currents for the two bilayer assemblies above agreed to within 12% and 8% with those calculated from eq 22, respectively.

(4) As shown in bilayer responses in Figures 3, 8, and 10, bilayer trapping and untrapping reaction peaks are nearly quantitative mirror images of one another.

(5) For the untrapping reaction peak of an electrode like that of Figure 11B, E_p was observed to vary with –0.066 log $\Gamma_{out(ox)(t=0)}$ over a range of (0.55–5.6) × 10^{-9} mol/cm^2 of trapped PVFer$^+$.

(6) Finally, we compare in Figure 13 (curves B and C) two experimental curves for outer-film untrapping of PVFer$^+$ states in a Pt/poly-VDQ^{2+}/PVFer bilayer with best-fit, calculated theoretical responses. The theoretical calculation depends on specifying values for $\Gamma_{VDQ} = \Gamma_{in(t=0)}$, $\Gamma_{PVFer} = \Gamma_{out(t=0)}$, and $E°_{VDQ}$, all independently measured quantities, and assuming no site interaction effects (r = 0). The theoretical response was then calculated by adjusting a single parameter, the product $k_{interf}\Gamma_{in(ox)(t=0)}^{interf}\Gamma_{out(red)(t=0)}^{interf}$ until an optimum match with experiment was obtained. The fit between theory and experiment is excellent for both electrodes shown.

Further examination of the electrochemical theory for bilayer action based on the rate law in eq 16 and on other alternative rate law statements is beyond the scope of this article and will be given elsewhere,[25] as will additional comparison to experimental results. To date, our studies of bilayer theory based on eq 16 indicate that it is a successful first step toward representing bilayer electrode behavior and can be employed for preliminary evaluations of k_{interf}.

Relationship of k_{interf} to Homogeneous Rates. The rate constant k_{interf} has unfamiliar dimensions, cm^2/(mol s), being an interfacial bimolecular reaction. It can be restated using more familiar units by rewriting eq 16 as eq 23, where C is concentration (mol/cm^3)

$$-dC_{out(red)}/dt = k_{homo}C_{in(ox)}C_{out(red)} \quad (23)$$

of the redox sites at the contacting interface and within the film and k_{homo} has the dimensions cm^3/(mol s). Equations 16 and 23 are connected by (film thickness) × $C = \Gamma_T$, which yields eq 24.

$$k_{homo} = k_{interf}\frac{\Gamma_{in(t=0)}^{interf}\Gamma_{out(t=0)}^{interf}}{C_{in(t=0)}\Gamma_{out(t=0)}} \quad (24)$$

From the result of Figure 13 that $k_{interf} = 10^{14}$ cm^2/(mol s), assuming $C_{in(t=0)} = 2 \times 10^{-3}$ mol/cm^3 for poly-VDQ^{2+} and assuming $\Gamma^{interf} \approx 2 \times 10^{-10}$, one calculates that $k_{homo} \approx 10^6$ cm^3/(mol s) or $\sim 10^3$ M^{-1} s^{-1} for this bilayer. It clearly will be of interest to compare such electron-exchange constants in the special environment of the inner/outer-film interface to homogeneous ones, but we will not consider this further here.

Theory for Reverse Electron-Transfer Reaction Leakage. Once an outer film has been oxidatively trapped and the electrode potential returned to a value quantitatively reducing the inner film, the back-reaction for the trapping reaction, e.g.

$$\text{inner(red)} + \text{outer(ox)} \rightarrow \text{inner(ox)} + \text{outer(red)} \quad (25)$$

becomes a possible leakage pathway for discharge of outer-film trapped states. This pathway is independent of applied potential as long as the inner film is quantitatively reduced. The leakage rate from reaction 25 is related to the trapping rate of reaction 16 by K_{eq}, obtained through $E°_{out} - E°_{in}$, and the initial current due to reaction 25 can be written as eq 26. The reverse electron-transfer pathway sets an upper boundary on lifetimes of trapped outer-film states, and eq 26 points out the importance

$$i_{L,c}/n_{ch}FA = \frac{-d\Gamma_{out(ox)}}{dt} = k_{interf}\exp\left[\frac{nF}{RT}(E°_{out} - E°_{in})\right][\Gamma_{in(red)(t=0)}^{interf}\Gamma_{out(ox)(t=0)}^{interf}] \quad (26)$$

(25) Denisevich, P.; Willman, K. W., University of North Carolina, 1980, to be submitted for publication.

of the difference $E^\circ_{out} - E^\circ_{in}$ in that regard. A calculation for the Pt/poly-Ru(VB)$_3^{2+}$/PVFer bilayer is instructive. If we take $E^\circ_{out} - E^\circ_{in}$ as −0.74 V and assume that $k_{interf} = 10^{12}$ cm^2/(mol s) and $\Gamma^{interf} \sim 2 \times 10^{-10}$ mol/cm^2, then the initial leakage rate of trapped outer-film PVFer$^+$ via reaction 25 is 1.2×10^{-20} mol/(cm^2 s) or a leakage current of 1×10^{-15} A/cm^2. With k_{interf} and $E^\circ_{out} - E^\circ_{in}$ of this magnitude, leakage by backreaction of the trapping reaction is not a serious determinant of trapped-state lifetimes.

Conclusions

Experimental results in this paper demonstrate the technical feasibility to assemble bilayers of redox substances which display more or less ideal rectifying and outer-film oxidation-state trapping and untrapping characteristics. The demonstration furthermore supports our assertion that the bilayer rectifying property depends on the particular characteristics of *redox conductivity* for electron flow across redox films as opposed to conventional concepts of electronic conductivity or semiconductor properties and is therefore new.

It now seems possible that a wide variety of redox materials will be adaptable to preparing bilayer electrodes. Further testing of redox materials for inner and outer films and of the characteristics of inner films in terms of leakage of outer-film trapped oxidation states is planned. This paper has identified three forms of trapped-state leakage: pinholes in the inner film (which preliminarily seem not to be catastrophic), reactivity toward trace oxidants or reductants in the solution (potentially of analytical advantage), and back-reaction of the trapping reaction (serious only when $E^\circ_{out} - E^\circ_{in}$ is small).

Leakage properties of bilayers constitute one important test of their ideality as rectifying and charge-trapping devices. The electrochemical potential and shape of the trapping and untrapping current peaks can provide additional criteria. The theory presented here is a first, and so far successful, step in accounting for bilayer voltammetric response which produced a preliminary value for the rate constant for electron transfer between inner- and outer-film redox sites at the film interface. There are numerous aspects of the theory and uncertainties in the experimental situation which remain to be tested or solved, an obvious one of which is the quantity of inner- and outer-film reactants present at (in) the inner/outer-film interface and participating in the trapping-electron exchanges.

Finally, we have said relatively little here about the potential analogies of bilayer electrodes to solid-state electronic devices. Figure 5 showed a diode-like bilayer current–voltage response, but many other characteristics are pertinent to this analogy, including switching time, charge capacity, and reproducibility of the bilayer diode potential. These and other chemical microelectronic possibilities of bilayer electrodes are under study and will be described in future articles.

Experimental Section

Preparation of the polymer modified electrode surfaces was as follows.

Pt/Poly-Ru(VB)$_3^{2+}$ was prepared as previously described,[2] by scanning the potential of a clean Pt electrode in a 0.1 M Et_4NClO_4/acetonitrile solution containing 0.1–0.5 mM [(4-vinyl-4′-methyl-2,2′-bipyridine)$_3$Ru](ClO$_4$)$_2$ repeatedly between 0 and −1.8 V vs. SSCE. The quantity of the polymerized form of this complex, poly-Ru(VB)$_3^{2+}$ which deposits on the Pt surface and gradually turns it yellow and then red-orange is systematically controllable by the details of the potential scanning program, monomer concentration, and solution agitation. For subsequent electrochemistry or electrochemical polymerization-coating experiments, the Pt/poly-Ru(VB)$_3^{2+}$ surfaces are simply rinsed with fresh acetonitrile and air-dried.

Pt/PVFer. Electrodes are coated with a 26 K polyvinylferrocene, PVFer, film by spreading and slowly evaporating 10–50 *m*L of a ca. 10^{-5} M (based on monomer) solution in toluene or CH_2Cl_2 on a clean, dry Pt disk.

Pt/Poly-VDQ^{2+}. A polymer film of the viologen "vinyldiquat", VDQ^{2+}, can be prepared by repeatedly scanning the Pt electrode potential between 0 and −1.2 V vs. SSCE (or by potentiostatting the electrode at −1.2 V) in an Et_4NClO_4/acetonitrile solution containing 1 mM 4-vinyl-4′-methyl-*N*,*N*′-ethylene-2,2′-bipyridinium hexafluorophosphate (VDQ^{2+}) monomer. Details of preparation of the monomer and of the electrochemistry of its polymerized films are given elsewhere.[19] The Pt/poly-VDQ^{2+} surface is washed with acetonitrile and air-dried.

Pt/Poly-BVSi^{2+}. The monomer *N*-methyl-*N*′-(4-(2-trimethoxysilyl)-ethyl)benzyl)-4,4′-bipyridinium dibromide, "benzylviologensilane", BVSi^{2+}, prepared by quaternizing *N*-methyl-4,4′-bipyridinium with 1-(trimethoxysilyl)-2-(*p*-chloromethyl)phenyl)ethane (Petrarch) as described elsewhere,[19] is dissolved in 4:1 CH_3CN/methanol, a few microliters of which are spread on the clean, dry Pt surface and allowed to slowly evaporate. Siloxane bond formation (polymerization) is aided in the dried film by heating in a vacuum oven at 50 °C for 60 min. Details of the electrochemical behavior of such polybenzylviologensilane (poly-BVSi^{2+}) films are described elsewhere.[19]

Pt/Poly-Ru(VB)$_3^{2+}$/PVFer, Pt/Poly-Ru(VB)$_3^{2+}$/Poly-BVSi^{2+}, Pt/Poly-VDQ^{2+}/PVFer, and Pt/Poly-BVSi^{2+}/PVFer. These bilayer electrodes were all made by first preparing the indicated inner film, air-drying, and then evaporating coating films of respectively PVFer and poly-BVSi^{2+} onto the inner layers in the same manner as the one-layer films of PVFer and poly-BVSi^{2+} described above were prepared.

Pt/Poly-Ru(VB)$_3^{2+}$/Poly-VDQ^{2+}. This bilayer electrode was fabricated by first coating with poly-Ru(VB)$_3^{2+}$ as above and then scanning the potential applied to this electrode in a 1 mM solution of vinyldiquat monomer repeatedly between 0 and −1.5 V vs. SSCE. No electrochemical wave at the potential for the divinylquat monomr is observed on the Pt/poly-Ru(VB)$_3^{2+}$ electrode; polymerization of vinyldiquat is initiated instead by reduction by the Pt/poly-Ru(VB)$_3^{+}$ surface which forms at −1.3 V.

Pt/Poly-Ru(VB)$_3^{2+}$/Poly-Fe(VB)$_3^{2+}$. This bilayer was prepared by first coating the electrode with poly-Ru(VB)$_3^{2+}$ as above and then scanning the potential applied to this electrode repeatedly between 0 and −1.8 V vs. SSCE in an acetonitrile solution of 0.1 mM [(4-vinyl-4′-methyl-2,2′-bipyridine)$_3$Fe](ClO$_4$)$_2$, Fe(VB)$_3^{2+}$. The polymerization of the Fe(VB)$_3^{2+}$ proceeds in a manner similar to that of Ru(VB)$_3^{2+}$ except that it is reduced indirectly by reducing the inner film to the poly-Ru(VB)$^+$ state.

Chemicals and Equipment. Chemicals are reagent grade or purified as in our earlier publications.[26] The *VB* ligand was a purified form.[2] Electrochemical equipment and cells are conventional. The Pt disk electrodes are shrouded with Teflon collars and before use are polished with 1-μm diamond paste. SnO_2 electrodes were highly doped films on glass as previously described.[26] X-ray photoelectron spectroscopy (XPS) was carried out with a Du Pont Model 650B electron spectrometer.

Acknowledgment. This research was supported by grants from the Office of Naval Research and the National Science Foundation. Assistance with XPS experiments was provided by Dr. M. Umaña. R. W. Murray acknowledges fellowship support from the Guggenheim Foundation and the hospitality of Stanford University during preparation of this article. This is paper 32 in a series of Chemically Modified Electrodes.

(26) Murray, R. W. *Acc. Chem. Res.* **1980**, *13*, 135.